Forming limit diagrams with an FE-based approach for sheets under non-proportional loading

A. Reyes[1], O. S. Hopperstad[1], T. Berstad[2,1], O.-G. Lademo[2,1]

[1] Strucural Impact Laboratory (SIMLab) - Centre for Research-based Innovation and

Department of Structural Engineering, Norwegian University of Science and Technology,

N-7491 Trondheim, Norway

[2] SINTEF Materials and Chemistry, N-7465 Trondheim, Norway

Summary:

In this study, LS-DYNA was used to predict the experimental forming limit diagrams (FLDs) for pre-strained sheets in aluminum alloy Al2008-T4 found by Graf and Hosford [1]. The original data of Graf and Hosford [1] includes numerous pre-straining situations, but it was here chosen only to investigate pre-straining by biaxial and uniaxial tension. In order to generate the FLDs, several analyses of a square patch were run systematically to construct the different points. Pre-straining was applied by first stretching a somewhat larger patch to a given pre-strain, and then trimming this patch to the standard square patch. The material model used in the analyses includes two instability criteria; a non-local criterion to detect incipient localized necking and a through-thickness shear instability criterion [2-5]. The objective was to study whether the effects of pre-straining on the FLD could be predicted by the chosen modelling approach, and good results were obtained.

Keywords: FE-based M-K analysis, Strain-path change, Forming limit diagrams

1 Introduction

Forming limit diagrams (FLDs) are regularly used to represent sheet formability, and describe the strain combinations (ε_1-ε_2) that lead to failure by local necking and possibly local fracture. Traditionally, FLDs have been found by physical tests, or analytically with the Marciniak-Kuczynski (M-K) method [6]. Furthermore, many numerical FLD-analyses have been based on the M-K method [4, 5, 7, 8].

The influence of strain-path change on FLDs has been a challenge as strain limits can be either raised or lowered depending on the nature of the strain-path change. Two similar experimental programs where the influence of changes in strain path was thoroughly investigated were carried out by Graf and Hosford for the aluminum alloys Al2008-T4 [1] and Al6111-T4 [9]. These studies showed that the amount of possible additional deformation after pre-straining depends on the effective strain during the pre-straining regardless of strain-path.

Berstad and Lademo et al. [2-5] have addressed how the loss of stability, as described by the classical analysis of Marciniak and Kuczynski, could be represented in non-linear shell-based finite element analyses with LS-DYNA. This FE-based approach is used in this study to represent the experimental FLDs for the pre-strained sheets of Al2008-T4 [1]. A more extensive study by Reyes et al. [10] includes also tests and the experimental results [9] of Al6111-T4. The tests of Graf and Hosford [1] included numerous pre-straining situations, but it was here chosen only to investigate pre-straining by biaxial and uniaxial tension. The material model used in the analysis includes two instability criteria; a non-local criterion to detect incipient localized necking and a through-thickness shear instability criterion.

2 FE-based M-K analysis

The FE-based M-K analysis can be used for automated calculation of FLDs of sheet materials [2-5, 11]. Several analyses of a square patch of n_{el} x n_{el} shell elements are run systematically in LS-DYNA to construct the different points in the FLD. The patch is subjected to proportional straining defined by a constant strain ratio $\rho=\Delta\varepsilon_y/\Delta\varepsilon_x$, and the strain ratio will be different for each run. A non-local instability criterion (NLIC) can be used with the material model, and localized necking is assumed to occur when this criterion is fulfilled during several consecutive steps. In order to initiate necking in the patch, an initial inhomogeneity, is needed. This is here introduced through the thickness, i.e. the nodal thickness (t) is given a random normal distribution where the mean value t_0 is typically the nominal thickness of the sheet. The coefficient of variation $CoV(t)=\sigma_t/t_0$ is also given as input, where σ_t is the standard deviation. Furthermore, a through-thickness shear instability criterion (TTSIC) is included in the material model. When either of the criteria is fulfilled, the time is recorded, and mean strains are calculated based on the global deformation of the patch.

Pre-straining is obtained by stretching a patch that is somewhat larger than the FLD patch to a given pre-strain. This patch is then trimmed to the standard patch size, and the history variables are mapped onto the new mesh. This was convenient in order to automate the procedure. The forming limit diagram of the pre-strained patch is then found by the FE-based M-K analysis on the new patch.

3 Material modeling

The Weak Texture Model (WTM) which is now available as material model No. 135 in LS-DYNA was used in this study. It is suitable for aluminium and the material parameters can be found from *R*-values and stress-strain data from uniaxial tensile tests in three directions, which are available in the study of Graf and Hosford [1]. The model and the procedure for identifying its parameters is thoroughly described by Lademo et al. [4, 5] and Reyes et al. [11].

Included in the model are isotropic elasticity, an anisotropic yield criterion (*Yld89* [12]), associated flow rule, combined non-linear isotropic and kinematic strain hardening, strain-rate hardening, and a few optional fracture criteria where one is the through-thickness shear instability criterion (TTSIC) [13, 14]. Kinematic hardening and strain-rate hardening were not used in the current investigation.

Yld89 [12] reads

$$a\left|K_1+K_2\right|^m+a\left|K_1-K_2\right|^m+c\left|2K_2\right|^m=2f^m \quad \text{where} \quad K_1=\frac{\sigma_x+h\sigma_y}{2}, \quad K_2=\sqrt{\left(\frac{\sigma_x-h\sigma_y}{2}\right)^2+\left(p\sigma_{xy}\right)^2} \tag{1}$$

(σ_x, σ_y, σ_{xy}) are the non-zero components of $\boldsymbol{\sigma}$ in plane stress states, where the *x*- and *y*-direction follow the axes of orthotropic symmetry. The rolling direction (RD) is here taken as the *x*-direction while the transverse direction (TD) is taken as the *y*-direction. The constants *a*, *c*, *h*, and *p* can be determined from experiments. The exponent *m* can typically be 6 for bcc materials and 8 for fcc materials, but can also be determined from experimental data or polycrystalline analyses [12].

In the present work, non-linear isotropic strain hardening is assumed, with the flow stress expressed by the extended Voce rule where Q_i and C_i are material constants:

$$\sigma_Y(\bar{\varepsilon})=\sigma_0+R(\bar{\varepsilon})=\sigma_0+\sum_{i=1}^{2}Q_i\left[1-\exp\left(-C_i\bar{\varepsilon}\right)\right] \tag{2}$$

A non-local value of the increment in plastic thickness strain is defined within a user-defined radius R_Ω. The radius was here assumed to include the whole patch, and the non-local value can be written as

$$\Delta\varepsilon_z^{p\Omega}=\frac{1}{n_{el}}\sum_{i=1}^{n_{el}}\Delta\varepsilon_z^{p(i)} \tag{3}$$

where n_{el} is the number of elements in the patch and equal-sized elements are assumed. Localized necking is assumed to occur at a time t_{cr} if the ratio β_i of the local to non-local plastic thickness strain

increment for element *i* exceeds a critical value β_{cr} at t_{cr} and during n_{it} consecutive steps [15]. β_i is defined by

$$\beta_i = \frac{\Delta\varepsilon_z^{p(i)}}{\Delta\varepsilon_z^{p\Omega}} \tag{4}$$

Experimental observations show that several aluminum alloys can fail by shear localization through the thickness of the sheet, close to the direction of maximum shear stress [16, 17]. In order to account for the shear fracture mode in shell element analysis, a through-thickness shear instability criterion based on the work of Bressan and Williams [13] has been implemented in WTM. The criterion was originally developed for materials with normal anisotropy, and was found to give reasonable predictions of forming limits when compared with other methods and experimental data [13]. The criterion can be extended to account for orthotropic anisotropy of the sheet metal [14]:

$$\left(\sin^2\varphi\cos^2\theta - \cos^2\varphi\right)d\varepsilon_x^p + 2\sin^2\varphi\cos\theta\sin\theta d\varepsilon_{xy}^p + \left(\sin^2\varphi\sin^2\theta - \cos^2\varphi\right)d\varepsilon_y^p = 0 \tag{5}$$

where θ is the angle between the rolling direction and the direction of the major principal stress. For given values of the plastic strain increments and of the angle θ, Equation (5) may be solved for the inclination φ of the localization band. With these assumptions, it follows that the criterion for shear instability, $|\tau| \geq \tau_{cr}$, reads

$$\sigma_1 \geq \frac{2\tau_{cr}}{\sin 2\varphi} \tag{6}$$

which is the same result that was obtained for materials exhibiting planar isotropy [13]. Note: the assumption that the material characteristic τ_{cr} is an isotropic quantity is kept here, even for materials with planar anisotropy. Naturally this is a very simplified assumption since one can imagine several directional micro-structural features that might influence the tendency for shear-band formation. However, the material considered in this study has rather weak planar anisotropy, so the assumption seems justifiable in this case.

Several methods to determine τ_{cr} exist; a uniaxial tension test or a balanced biaxial test [13], or Hill's analysis of localized necking for negative strain ratios to determine τ_{cr} for plane strain [13] for which no additional tests are needed to identify the shear instability criterion.

More details about the material modeling is given by Reyes et al. [10].

4 Identification of parameters

Graf and Hosford [1] carried out standard uniaxial tensile tests in three different directions (0°, 45°, 90°) to the rolling direction, and the stress-strain data was fitted to the power-law hardening model

$$\bar{\sigma} = k\bar{\varepsilon}^n . \tag{7}$$

Furthermore, corresponding *R*-values are given by Graf and Hosford [1]. In order to identify the parameters in WTM, the power-law hardening curves for the 0°-direction were fitted to the extended Voce strain-hardening model in Equation (2). The parameters were found by fitting the model and test data through a least-square approach. The fitted true stress-strain curves are shown in Figure 1 (a), and only slight strength anisotropy is present for the materials.

The exponent *m* was taken as 8 for the yield criterion because Al2008 is a fcc sheet material. Additionally, the parameters *a*, *c*, *h*, and *p* were identified by means of the experimental *R*-values and flow-stress ratios, through minimizing the sum of squares between the model representation and the experimental data. The flow-stress ratio r_α is here defined as the ratio between the flow stress σ_α in one test and a reference flow stress σ_{ref} for the same amount of plastic work W_p. Flow-stress ratios for varying plastic work were calculated for each test, where the flow stress in one parallel in the 0°-direction was used as the reference flow stress. *R*-values and flow-stress ratios were found from the model using the identified parameters, and as one can see in Figure 1 (b), the flow-stress ratios are

predicted reasonably well, while the *R*-values are not that well described, especially for the 90°-direction. Plots of the identified yield surface are shown in Figure 2.

TTSIC was calibrated through inverse modeling in one step. The critical strain at plane strain conditions was found from the initial FLDs from Graf and Hosford [1]. A plane strain analysis of one element was run, and the shear stress on the critical plane was plotted vs. strain. The shear stress corresponding to the critical strain from the plane strain tests was taken as the critical shear stress in TTSIC. This critical strain in the rolling direction (RD) is somewhat higher than the critical strain in the transverse direction (TD), and because of this, analyses of plane strain in both the rolling and transverse direction were carried out. The critical shear stress was found to be 186 for RD and 184 for TD [10]. Note that even a small change in the critical value might have significant influence for a stress-based criterion such as TTSIC. However, the critical shear stress identified from RD was used in the subsequent numerical analyses.

More details about the identification procedure can be found in Reyes et al. [10].

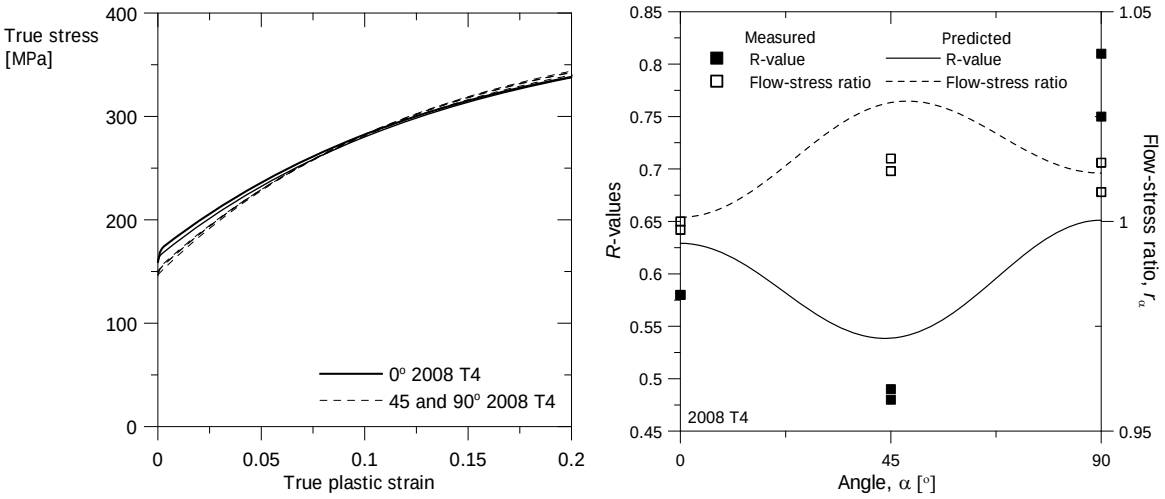

Figure 1: (a) True stress-strain curves of the aluminum alloys Al2008 T4. (b) Experimental and predicted R-values and flow-stress ratios vs. angle.

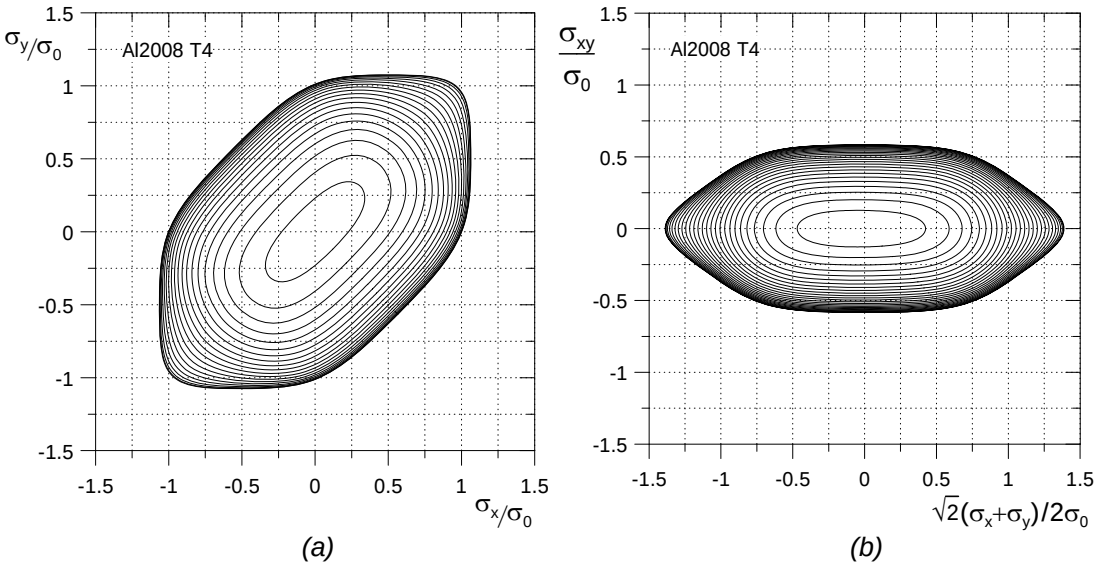

Figure 2: (a) Identified yield surfaces in the space of σ_x and σ_y (b) Yield loci defined by intersections of the yield surface and planes parallel to the plane $\sigma_x = \sigma_y$.

5 Forming limits

Forming limits were found by means of the FE-based M-K analysis. A patch of 60 x 60 mm^2 and 50 x 50 Belytschko-Tsay shell elements were stretched to a given pre-strain. A new, smaller patch of 50 x 50 mm^2, and 50 x 50 Belytschko-Tsay shell elements were then cut out of the pre-strained patch, and the forming limits were found from 26 different cases of proportional loading. The element thickness and history variables were mapped onto the new and smaller patch. In order to plot the final FLD, the pre-strains were added to the strains from the subsequent analyses. For comparison, the same procedure was followed to predict the FLDs for the as-received sheets; hence the pre-strain was set to zero.

The numerical parameter β_{cr} was set as 2, and n_{it} was set to 1000. For one case, n_{it} was increased to 1500 for some of the runs in the series of pre-strained sheets in uniaxial tension $\parallel$ RD to 18% (FLD $\perp$ RD). For a higher value of β_{cr} (e.g. 5-10), a lower value of n_{it} could be used.

Furthermore, a thickness variation following a Gaussian distribution was used, with the thickness of 1.05 mm as the mean value and the coefficient of variation of the thickness *CoV(t)* = 0.005. The thickness was actually not specified by Graf and Hosford [1], but it was chosen to use the same thickness as they used for Al6111 [9]. Note that the chosen procedure assigns a random thickness to each node, which means that numerical simulations with identical input will yield different results. The FLDs here are therefore only one realization of the given input. In order to make sure that the response is of wanted probability one could carry out several analyses with the same input. Fyllingen et al. [15] have recently looked into this matter, and found that the assumed thickness variations resulted in a quite wide scatter band.

Due to the presence of anisotropy 'full' FLDs were found as they are not generally symmetric about the axis of balanced biaxial straining, i.e. the axis defined by $\varepsilon_x = \varepsilon_y$. In the case of pre-strain, possible growth of directional inhomogeneity that depends on the pre-strain mode and the constitutive response can occur.

For more details, see Reyes et al. [10].

5.1 FLDs for as-received sheets

The predicted FLDs for the as-received sheets are shown in Figure 3, together with the test results of Graf and Hosford [1]. NLIC over-predicts the formability, while TTSIC is conservative and gives the best result compared to the experiments. In this case the FLD is almost symmetric about the axis of balanced biaxial deformation.

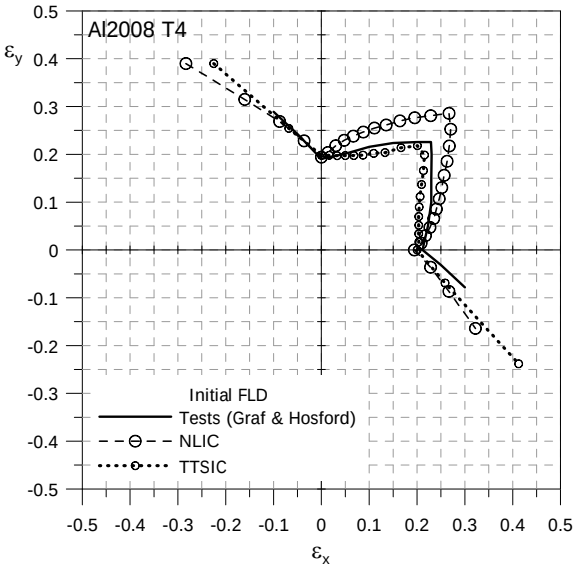

Figure 3 FLDs for as-received sheets; tests [1] *and numerical analyses* [10].

5.2 Biaxial pre-strain

The patch was stretched to the same amount of strain in both the *x*- and *y*-direction in order to obtain biaxial pre-strains. Resulting forming limits were predicted after pre-stretching by the FE-based M-K approach. The pre-strain was then added to the strains from the simulations (the strain in the *x*- and *y*-direction was the same in this case). The test results of Graf and Hosford [1] are given in Figure 4 *(a)* together with the predicted forming limits from the model with both NLIC *(c)* and TTSIC *(d).* For better readability, only the "upper part" of the forming limit curves is shown. Pre-strains are indicated with arrows in the diagrams. The trends for the tests and analyses are similar for both instability criteria. As an example, Figure 4 *(b)* compares the results from the different criteria for a pre-strain of 7%. This comparison is quite representative for all pre-strains.

All in all, both instability criteria can describe the behavior quite well as the governing phenomenon is plastic instability. That is, the localized necking process is initiated prior to the satisfaction of either instability criteria and the potential difference between the critical principal strains for the two criteria is thus limited. One has to expect some discrepancy between the FLDs for the pre-strained sheets as there is also some discrepancy between the experimental and predicted FLDs for the as-received materials.

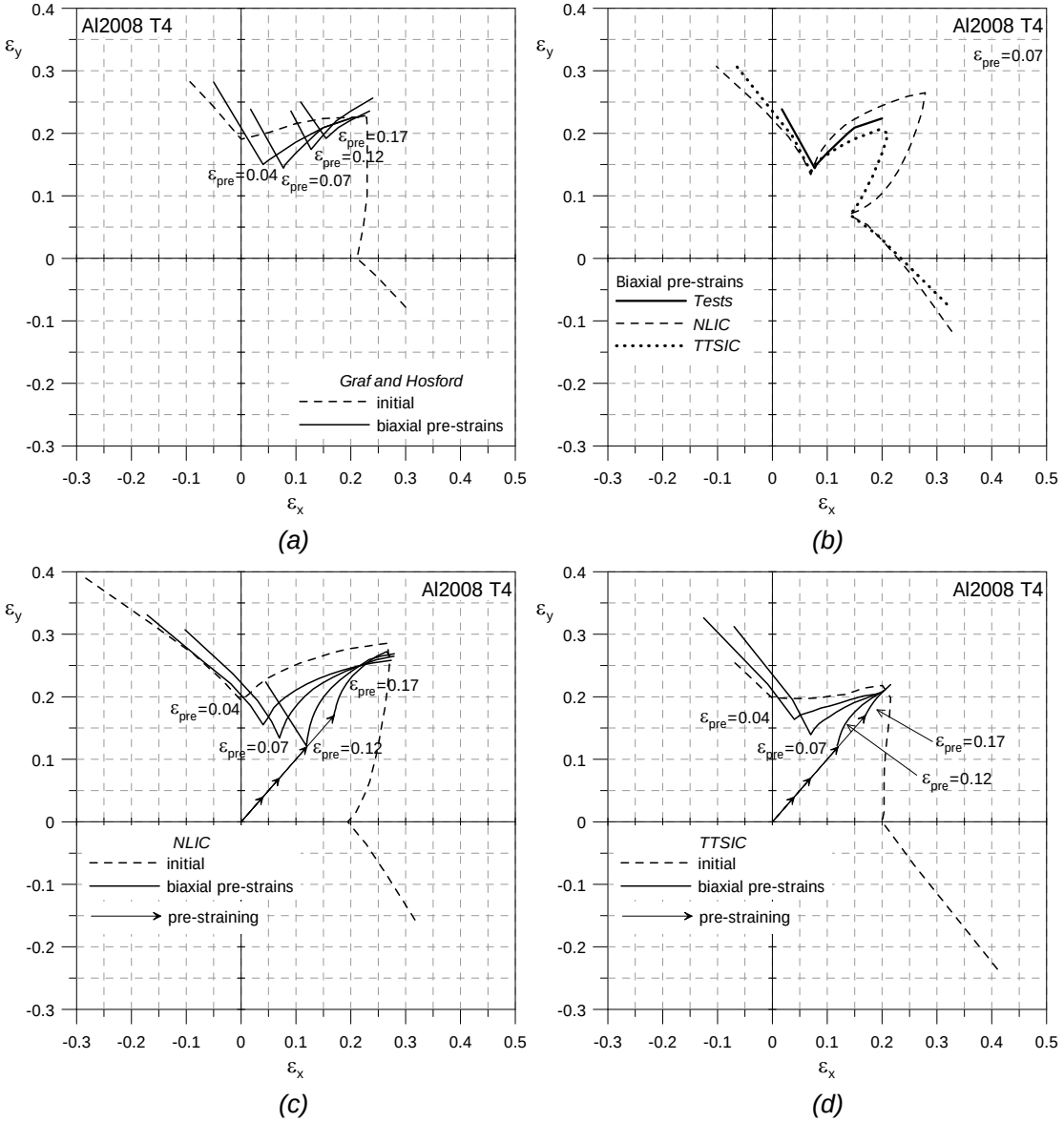

Figure 4 FLDs for biaxial pre-strains; (a) all pre-strains from tests [9] *(b) comparison between the FLDs from tests* [1] *and analyses* [10] *for a biaxial pre-strain of 7% (c) and (d) all pre-strains from numerical analyses* [10] *with NLIC (c) and TTSIC (d).*

5.3 Pre-straining by uniaxial tension

Pre-straining by uniaxial tension was obtained by stretching the patch to a certain amount of strain in one direction with no constraints in the other direction. After pre-stretching, resulting forming limits were predicted by the FE-based M-K approach. As for the biaxial pre-straining, the pre-strains were then added to the strains from these analyses. The resulting pre-strain in the transverse direction was found by measuring the corresponding length of the patch after pre-straining.

5.3.1 Pre-strain ⊥ RD - FLD ⊥ RD

Several cases of pre-straining by uniaxial tension were tested by Graf and Hosford [1]. In the first case, pre-strains were applied normal to RD and the FLD-tests were conducted so that the largest strain was normal to RD. The same procedure was followed in the numerical analyses. The test results of Graf and Hosford [1] are given in Figure 5 *(a)* together with the predicted forming limits with the two instability criteria *(c)-(d)*, while the FLDs (test and predicted) for 18% pre-strain are compared in Figure 5 *(b)*.

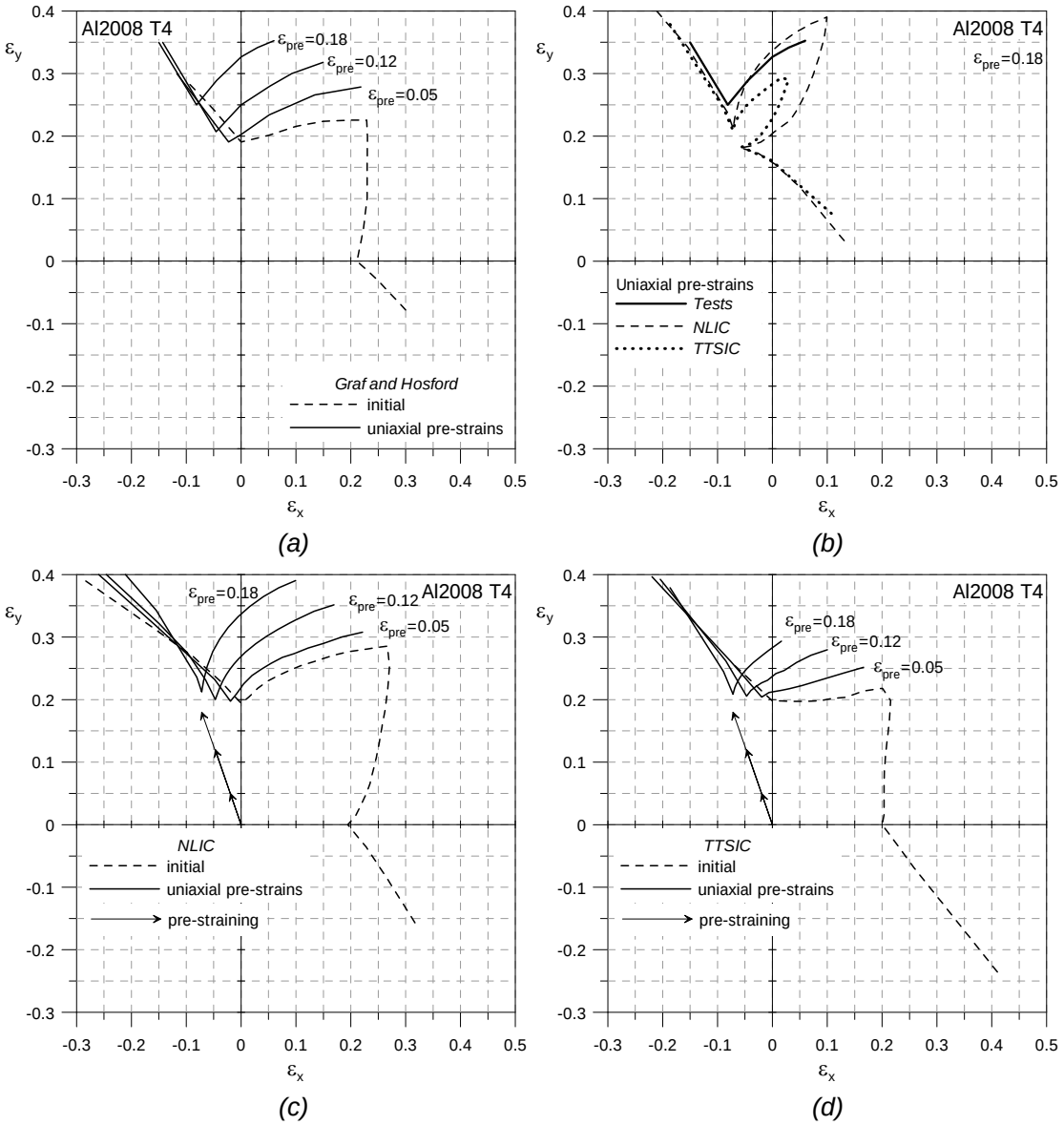

Figure 5 FLDs for pre-strains by uniaxial tension (pre-strain ⊥ RD, FLD ⊥ RD); (a) all pre-strains from tests [9] *(b) comparison between the FLDs from tests* [1] *and analyses* [10] *for a uniaxial pre-strain of 18% (c) and (d) all pre-strains from numerical analyses* [10] *with NLIC (c) and TTSIC (d).*

5.3.2 Pre-strain ⊥ RD -FLD // RD

Another case of forming limits was found as the specimen was pre-strained by uniaxial tension normal to RD and the largest strain in the FLD-tests was parallel to RD [1]. The test results of Graf and Hosford [1] are given in Figure 6 (a) together with the predicted forming limits (c)-(d), and in Figure 6 (b) the FLDs for the different criteria are compared with the test results for 12 % pre-strain. Note that ε_x and ε_y, in this case, are represented respectively by the ordinate and abscissa.

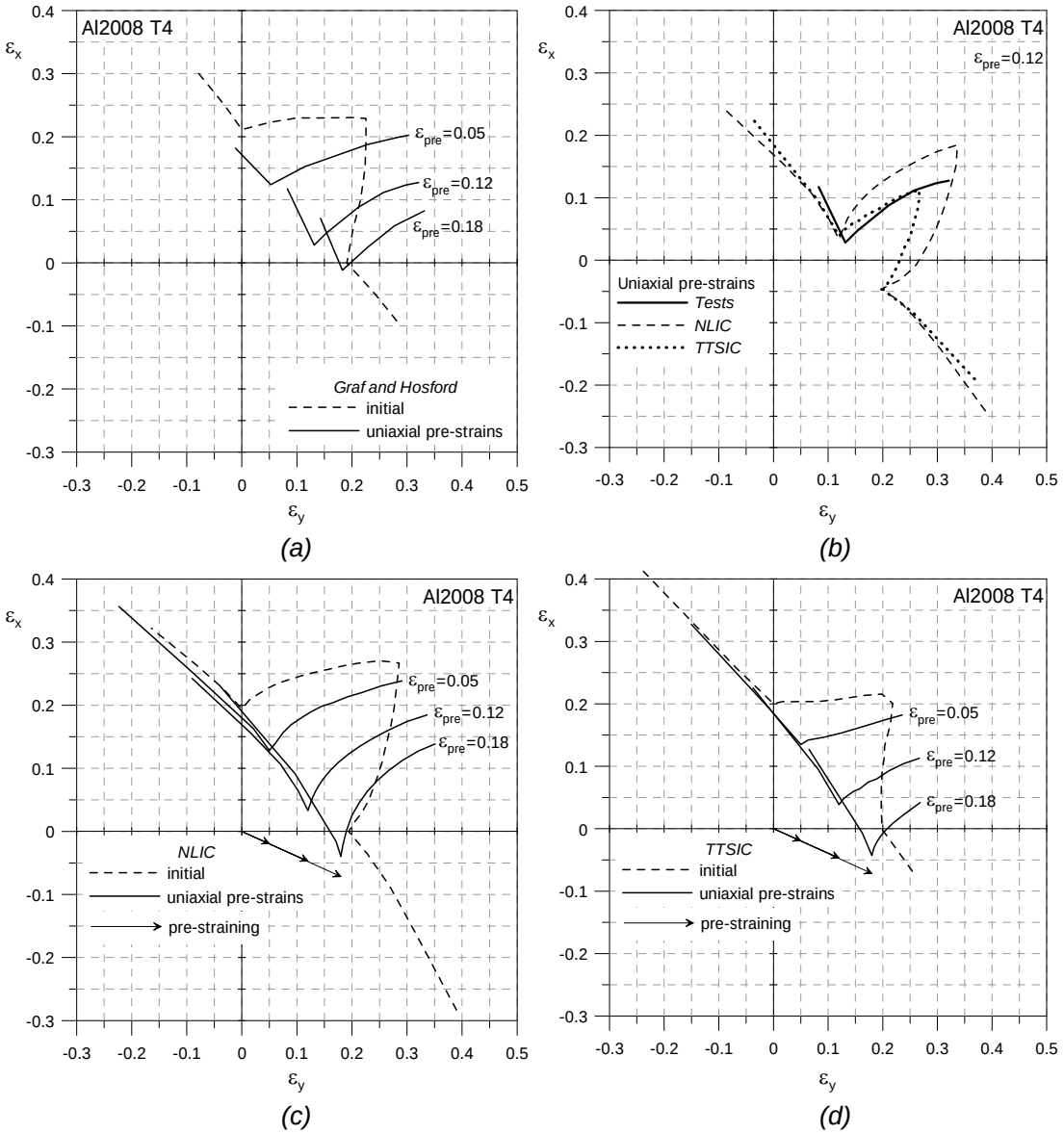

Figure 6 FLDs for pre-strains by uniaxial tension (pre-strain ⊥ RD, FLD // RD); (a) all pre-strains from tests [9] *(b) comparison between the FLDs from tests* [1] *and analyses* [10] *for a uniaxial pre-strain of 12% (c) and (d) all pre-strains from numerical analyses* [10] *with NLIC (c) and TTSIC (d).*

5.3.3 Pre-strain // RD, FLD ⊥ RD

In the third case of pre-straining by uniaxial tension, the pre-strains were applied parallel to RD while the largest strain was normal to RD in the FLD-tests. The same procedure was followed in the analyses. The test results of Graf and Hosford [1] are given in Figure 7 (a) together with the predicted forming limits (c)-(d), while Figure 7 (b) compare the FLDs predicted with the different instability criteria for 12.5 % pre-strain.

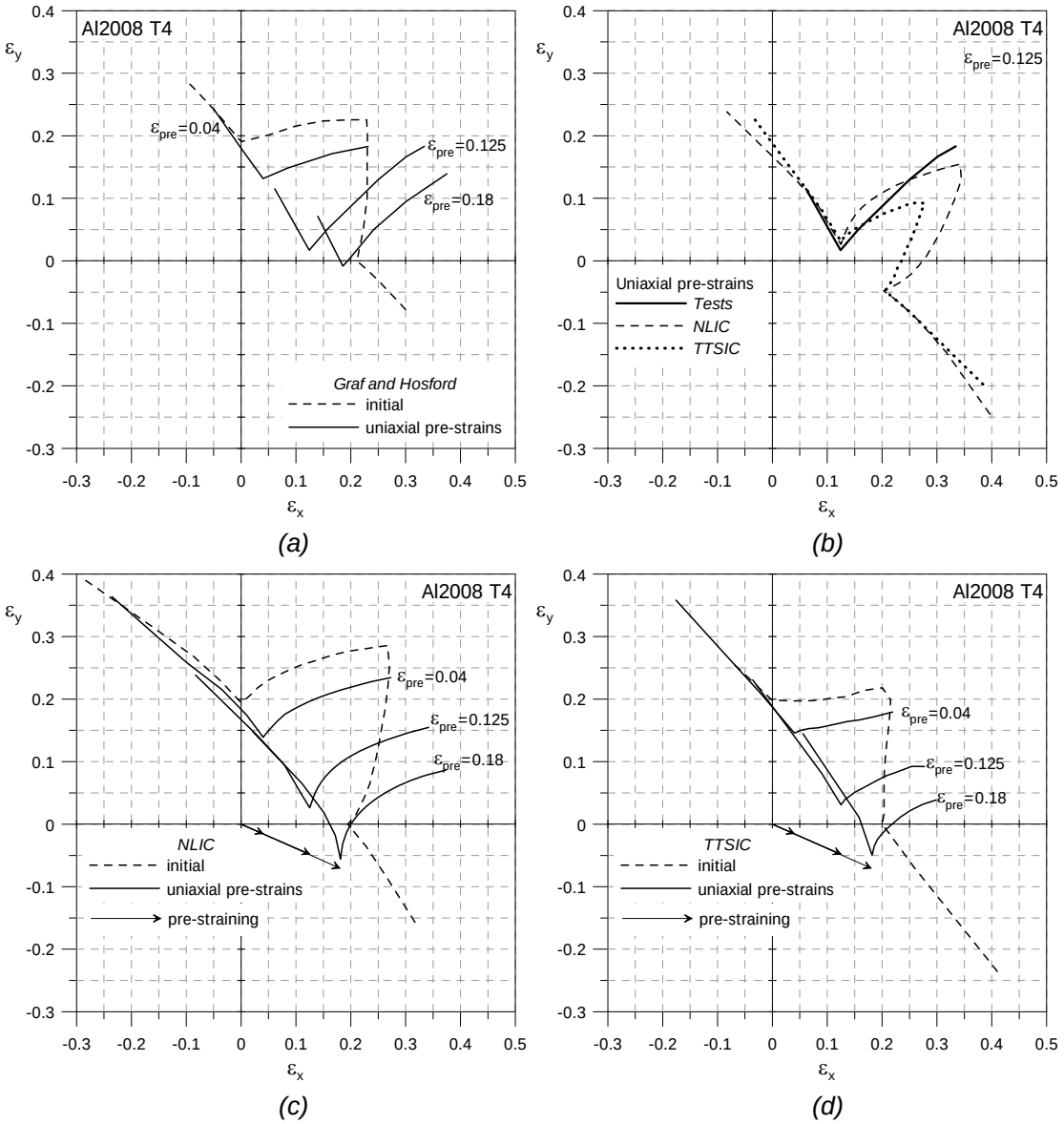

Figure 7 FLDs for pre-strains by uniaxial tension (pre-strain ∥ RD, FLD ⊥ RD); (a) all pre-strains from tests [9] *(b) comparison between the FLDs from tests* [1] *and analyses* [10] *for a uniaxial pre-strain of 12% (c) and (d) all pre-strains from numerical analyses* [10] *with NLIC (c) and TTSIC (d).*

The trends for the tests and analyses are comparable in all three cases of uniaxial pre-strain. In the first case however, the *y*-strain at the minimum point increases for increasing pre-strain in the tests, while it remains more or less constant for the analyses. Stoughton [18] observed the same, and concluded that there could be some uncertainties in the experimental data. It is clear the exact test results could not be reproduced, but both instability criteria can describe the behavior quite well, and take turns in predicting FLDs closest to the test results [10]. As mentioned earlier, this is due to the fact that the governing phenomenon is plastic instability. It should be noted that the predicted full FLDs after the pre-strain in uniaxial tension are highly unsymmetrical, at least with respect to the axis $\varepsilon_x = \varepsilon_y$.

The good agreement between the predicted and experimental FLDs for pre-straining in both biaxial and uniaxial tension indicates that the chosen shell element modeling technique, constitutive model and parameter identification procedure are capable of representing the onset of plastic instability also as function of these non-proportional loading paths. It is noteworthy that the agreement has been achieved without introduction of the kinematic hardening, i.e. by the simple means of isotropic hardening.

6 Conclusions

The non-linear FE-simulations with shell elements and assumptions of isotropic hardening and an anisotropic yield criterion with a small inhomogeneity were able to capture the strong strain-path dependence observed in the experiments. Additionally, the two instability criteria performed in consistency with each other and the experimental data. The results are promising for the use of the same FE-modeling procedure and material model in prediction of plastic instability in large scale simulations of components and structures subjected to general loading paths e.g. as in forming operations or crash events.

7 Acknowledgements

The present work was carried out with financial support from the Faculty of Engineering Science and Technology, Norwegian University of Science and Technology (NTNU), the Research Council of Norway, Renault, Fondation Franco-Norvégienne, and Hydro Aluminium Structures.

8 Literature

[1] Graf, A & Hosford, W: "Effect of Changing Strain Paths on Forming Limit Diagrams of Al 2008-T4", Metallurgical Transactions A, 24, 1993, 2503-2512

[2] Berstad, T, Lademo, O-G & Pedersen, KO: "Formability modeling with LS-DYNA" In: 8th LS-DYNA International Users Conference, 2-4 May, 2004

[3] Berstad, T, Hopperstad, OS & Lademo, O-G: "FLD calculator - a tool for calculation of foming limit diagrams with LS-DYNA", Report No. STF24 F02285 (Proprietary), 2002

[4] Lademo, O-G, Berstad, T, Hopperstad, OS & Pedersen, KO: "A numerical tool for formability analysis of aluminium alloys. Part I: Theory", Steel Grips, 2, 2004, 427-431

[5] Lademo, O-G, Pedersen, KO, Berstad, T & Hopperstad, OS: "A numerical tool for formability analysis of aluminium alloys. Part II: Experimental validation", Steel Grips, 2, 2004, 433-437

[6] Marciniak, Z & Kuczynski, K: "Limit strains in the process of stretch-forming sheet metal", International Journal of Mechanical Sciences, 9, 1967, 600-620

[7] Samuel, M: "Numerical and experimental investigations of forming limit diagrams in metal sheets", Journal of Materials Processing Technology, 153-154 (1-3), 2004, 424-431

[8] Abedrabbo, N, Pourboghrat, F & Carsley, J: "Forming of aluminum alloys at elevated temperatures - Part 2: Numerical modeling and experimental verification", International Journal of Plasticity, 22 (2), 2006, 342-373

[9] Graf, A & Hosford, W: "Influence of strain-path changes on forming limit diagrams of Al 6111 T4", International Journal of Mechanical Sciences, 36 (10), 1994, 897-8910

[10] Reyes, A, Hopperstad, O, Berstad, T & Lademo, O-G: "Prediction of necking for two aluminum alloys under non-proportional loading by using an FE-based approach", International Journal of Material Forming, 1 (4), 2008, 211-232

[11] Reyes, A, Hopperstad, OS, Lademo, O-G & Langseth, M: "Modeling of textured aluminum alloys used in a bumper system: Material tests and characterization", Computational Materials Science, 37 (3), 2006, 246-268

[12] Barlat, F & Lian, J: "Plastic behavior and stretchability of sheet metals. Part I: A yield function for orthotropic sheets under plane stress conditions", International Journal of Plasticity, 5, 1989, 51-66

[13] Bressan, JD & Williams, JA: "The use of a shear instability criterion to predict local necking in sheet metal deformation", International Journal of Mechanical Sciences, 25 (3), 1983, 155-168

[14] Hopperstad, OS, Berstad, T, Lademo, O-G & Langseth, M: "Shear instability criterion for plastic anisotropy", Report no STF80MK F06087, 2006

[15] Fyllingen, Ø, Hopperstad, OS, Lademo, O-G & Langseth, M: "Estimation of forming limit diagrams by use of the finite element method and Monte Carlo simulation", Computers and Structures, 87 (1-2), 2009, 128-139

[16] Lademo, O-G: "Engineering models of elastoplasticity and fracture for aluminium alloys", Doctoral thesis, 1999

[17] Hooputra, H, Gese, H, Dell, H & Werner, H: "A comprehensive failure model for crashworthiness simulation of aluminium extrusions", International Journal of Crashworthiness, 9 (5), 2004, 449-464

[18] Stoughton, TB: "General forming limit criterion for sheet metal forming", International Journal of Mechanical Sciences, 42 (1), 2000, 1-17